SUPPLEMENTARY MATERIAL

Integrated Computational Fluid Dynamics and Experimental Evaluation of a Tubular Membrane Photoreactor for UVC-Driven Advanced Oxidation at Bench- and Pilot-Scale

Carla S. Santos[a], Paulo H. Marrocos[a], Claudio Passalía[b], Marisol D. Labas[b,c], Rodolfo J. Brandi[b,c], Rosa Montes[d], Rosario Rodil[d], José B. Quintana[d], Ana I. Gomes[a], Vítor J.P. Vilar[a*]

[a] *LSRE-LCM, ALiCE, Faculty of Engineering, University of Porto, Rua Dr. Roberto Frias, 4200-465 Porto, Portugal*

[b] *Departamento de Medio Ambiente, Facultad de Ingeniería y Ciencias Hídricas, Universidad Nacional del Litoral FICH/UNL, Santa Fe, Argentina*

[c] *Instituto de Desarrollo Tecnológico para la Industria Química - INTEC (CONICET/UNL), Güemes 3450, Santa Fe, Argentina*

[d] *Aquatic One Health Research Center (ARCUS) & Department of Analytical Chemistry, Nutrition and Food Sciences, R. Constantino Candeira S/N, IIAA building, Universidade de Santiago de Compostela, 15782, Santiago de Compostela, Spain*

[*]Corresponding authors:

Tel.: +351 918257824; E-mail: anaisa@fe.up.pt (Ana I. Gomes); vilar@fe.up.pt (Vítor J.P. Vilar)

MATERIALS AND METHODS

MIRO®4 UVC aluminum foil

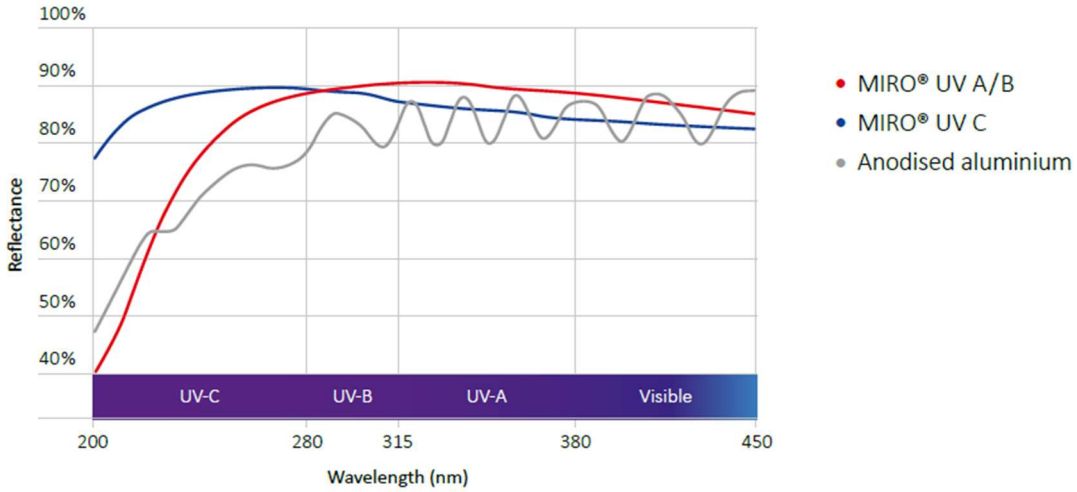

Figure SM-1. Reflectance of MIRO®4 UVC aluminum foil according to the wavelength.

Actinometric determinations

Actinometric tests were conducted using a circulating ferrioxalate solution in the ARZ, following the methodology described by Martín-Sómer et al. [1]. For bench-scale actinometric tests, the actinometric solution was prepared by dissolving 2.27 g of oxalic acid dihydrate ($C_2H_2O_4 \cdot 2H_2O_2$) in demineralized water (DW) to obtain a final oxalic acid concentration of 18 mM. Then, it was added 1.47 g of ferric sulfate pentahydrate ($Fe_2(SO_4)_3 \cdot 5H_2O$), resulting in a ferric ions (Fe^{3+}) concentration of 6 mM, along with 100 mL of 1 N sulfuric acid (H_2SO_4), yielding aa total solution volume of 1 L. The reagent quantities were doubled for the pilot-scale actinometric measurements to achieve a final volume of 2 L.

The generation of ferrous ions (Fe^{2+}) during irradiation was tracked through the formation of a tris-phenanthroline complex, which exhibits an orange color. This was achieved by mixing 0.25 mL of the sample with 2.5 mL of a buffer solution (prepared by dissolving 54.18 g of sodium acetate trihydrate ($C_2H_3NaO_2 \cdot 3H_2O$) and 5 mL of 96% pure H_2SO_4 in 500 mL of DW), followed by the addition of 6.25 mL of H_2O and 1 mL of a 1,10-phenanthroline ($C_{12}H_8N_2$) solution (1 g L^{-1}). The absorbance of the complex was recorded at 510 nm using a VWR UV-6300PC spectrophotometer.

The concentration of Fe^{2+} formed during the irradiation period was determined from the slope of the Fe^{2+} concentration (mol L^{-1}) *vs*. time (s), assuming up to 25% ferrioxalate degradation. This value was then multiplied by the total volume of the actinometric solution and Avogadro's number to estimate the number of Fe^{2+} ions produced. The radiation power reaching the reactor was calculated according to Eq. 1.

$$\text{Radiation Power} = \frac{k\,\text{NA}}{\varphi_{254}} \cdot \frac{h\,\text{c}}{\lambda} \qquad \text{(Eq. 1)}$$

Where k is the slope of Fe^{2+} concentration (mol s^{-1}), NA is the Avogadro's number (6.02 $\times 10^{23}$ mol^{-1}), φ_{254} is the quantum efficiency at 254 nm (1.38), h is Plank's constant (6.63 $\times 10^{-34}$ J s), c is the speed of light in a vacuum (3.00 $\times 10^{8}$ m s^{-1}) and λ is the wavelength (2.54 $\times 10^{-7}$ m).

Analytical Methods, instrumentation, and characterization of the CAS effluent

Table SM-1. Analytical determinations/equipment employed and characterization of the CAS effluent.

Parameter	Methodology/Equipment	Units	CAS effluent
pH	Hanna Instruments HI8424	-	7.7
Conductivity	Hanna Instruments Edge HI2003-02	$\mu S\ cm^{-1}$	1606
Absorbance UV_{254}	Merck Spectroquant® Prove 300 UV/Vis spectrophotometer	cm^{-1}	0.287
Chemical Oxygen Demand (COD)	Dichromate closed reflux method according to the 5220 D test [2]	$mg\ L^{-1}$	93.8
Dissolved Organic Carbon (DOC)	Non-dispersive infrared (NDIR) spectrometry in a TOC-V_{CSN} analyzer from Shimadzu	$mg\ L^{-1}$	12.8
Dissolved Inorganic Carbon (DIC)		$mg\ L^{-1}$	84.5
Total Suspended Solids (TSS)	According to the 2540 D and 2540C test [2]	$mg\ L^{-1}$	22.8
Chloride (Cl^-)	Dissolved inorganic anions were analyzed by ion chromatography in a Dionex ICS-2100 LC equipped with an IonPac® AS11-HC 250 mm × 4 mm column (T = 30 ºC) and a self-regenerating anion suppressor (ASRS® 300, 4 mm) under an isocratic elution of 30 mM KOH at a flow rate of 1.5 mL min^{-1}.	$mg\ L^{-1}$	179
Nitrate (NO_3^-)		$mg\ L^{-1}$	<0.03
Nitrite (NO_2^-)		$mg\ L^{-1}$	8.04
Sulfate (SO_4^{2-})		$mg\ L^{-1}$	48.7
Phosphate (PO_4^{3-})		$mg\ L^{-1}$	22.9
Ammonium (NH_4^+)	Dissolved inorganic cations were evaluated by ion chromatography in a Dionex AquionTM coupled with an IonPac® CS12A 250 mm × 4 mm column at ambient temperature and a CSRS® Ultra II cation self-regenerating suppressor (4 mm) under an isocratic elution of 20 mM methanesulfonic acid at a flow rate of 1.0 mL min^{-1}	$mg\ L^{-1}$	107
Potassium (K^+)		$mg\ L^{-1}$	31.3
Sodium (Na^+)		$mg\ L^{-1}$	139
Calcium (Ca^{2+})		$mg\ L^{-1}$	28.0
Magnesium (Mg^{2+})		$mg\ L^{-1}$	9.32

VLX analysis – Pilot-scale tubular membrane photoreactor

In the pilot-scale treatment tests, VLX was used as the model OMP. High-Performance Liquid Chromatography (HPLC) was performed with a VWR-Hitachi LaChrom Elite® liquid chromatograph, which was equipped with a Merck Purospher STAR RP-18 column and an L-2455 diode array detector (DAD) set to a wavelength of 225 nm. An isocratic elution was utilized, with a mixture of 40% 0.010 M oxalic acid and 60% methanol (v/v). The flow rate was maintained at 0.6 mL min^{-1}, and the injection volume was 40 µL. The total run time was 7 minutes, with a retention time of 3.4 minutes. The methods were validated by assessing linearity (R^2, 0.998) alongside the limit of quantification (LOQ, 2.52 mg L^{-1}) and limit of detection (LOD, 0.76 mg L^{-1}).

Mesh independence study

A grid independence study was performed considering representative variables from the velocity, species, and radiation fields. For the hydrodynamic field, the velocity magnitude, as well as the axial and radial velocity components, were evaluated as cross-sectional averages at the mid-length of the reactor. The number of mesh elements was progressively increased until these quantities became independent of further mesh refinement (the variations did not exceed 2.3%). Regarding species transport, the peroxydisulfate (PDS) concentration at the outlet, the concentration at an intermediate cross-section of the reactor, and the ratio between both concentrations were selected as representative parameters. These analyses were carried out under non-reactive conditions. While local concentration values, particularly near the membrane, showed some sensitivity to mesh refinement due to the use of an effective diffusion coefficient, the selected integral metrics converged to stable values as the mesh was refined. In particular, outlet concentrations and concentration ratios exhibited variations below 1.2% upon further refinement, indicating effective grid independence for the quantities relevant to reactor performance. For the radiation field, in addition to ensuring a sufficiently refined spatial mesh to resolve local gradients, the average incident radiation (irradiance) on the reactor wall and on the reflector surface was used as the representative parameter. Furthermore, the dominant factor governing solution accuracy was the angular discretization of the radiative intensity within the Discrete Ordinates Method. The number of discrete directions per hemispherical solid angle was therefore used as the controlling parameter. It was found that, for angular discretizations between 14 × 14 and 16 × 16 directions per hemisphere, both the radiation field and the corresponding surface-averaged irradiance values became independent of further angular refinement, as the incident radiation of the reflective wall varied less than 0.06%.

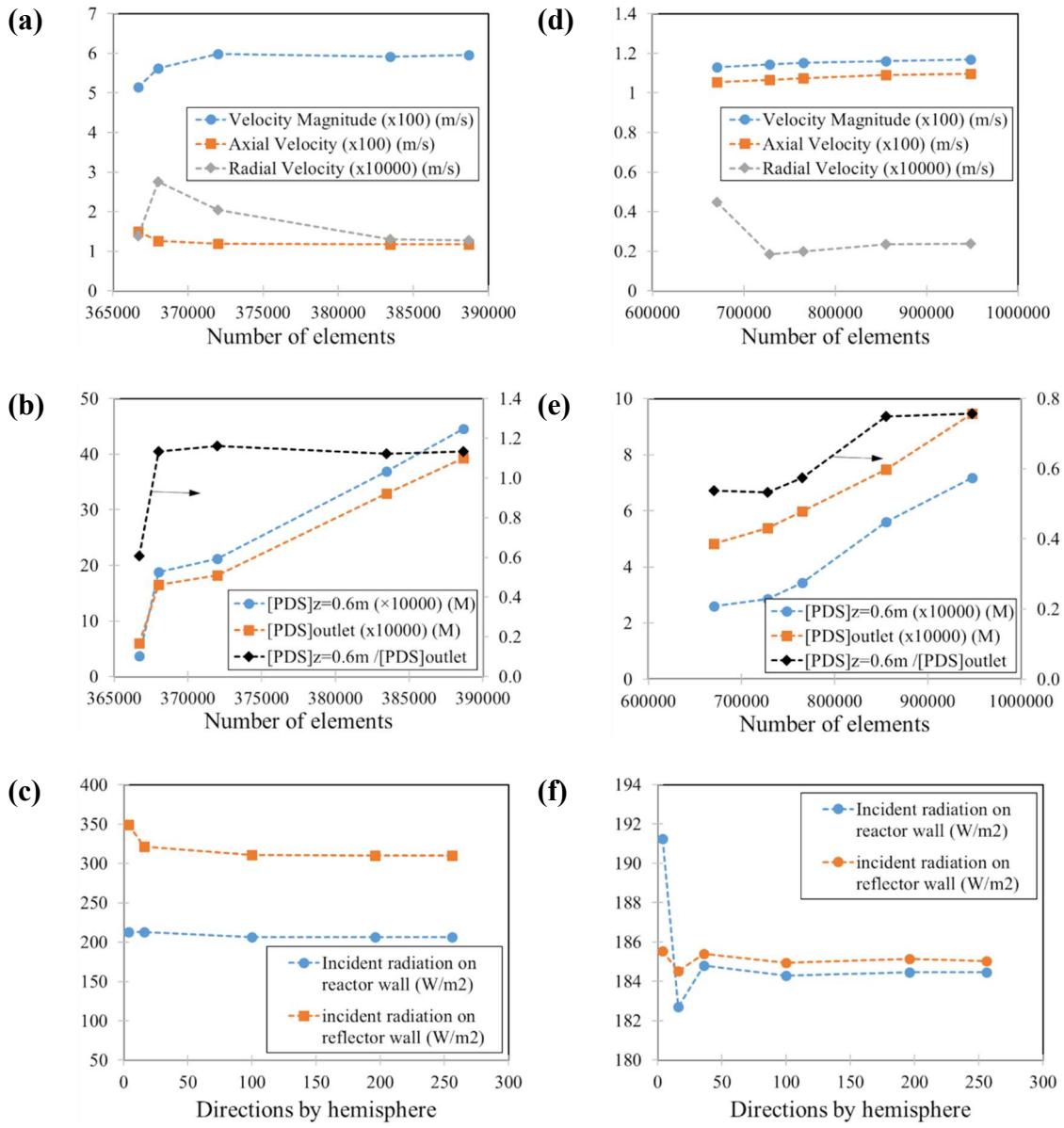

Figure SM-2. Mesh and angular discretization independence study for the tubular membrane photoreactor at bench scale (a - c) and pilot scale (d - f). (a, d) Variation of velocity magnitude, axial velocity, and radial velocity as a function of the number of mesh elements; (b, e) Effect of mesh refinement on persulfate (PDS) concentration at z = 0.6 m, at the reactor outlet, and the concentration ratio ($[PDS]_{z=0.6\ m}$ /$[PDS]_{outlet}$); (c, f) Influence of angular discretization in the Discrete Ordinates (DO) radiation model, expressed as the number of directions per hemisphere, on the incident radiation at the reactor and reflector walls.

Table SM-2. Boundary conditions

Item		Boundary condition	
		Bench-scale	**Pilot-scale**
Velocity field	Fluid velocity inlet (m s^{-1})	0.4	0.3
	Inlet volumetric flow rate (m^3 s^{-1})	8.339×10^{-6}	8.333×10^{-6}
	Outlet pressure	Zero-gauge	Zero-gauge
	Solid walls	No-slip	No-slip
	Initial fluid conditions	At rest at zero-gauge pressure and 20 ºC (isothermal conditions)	At rest at zero-gauge pressure and 20 ºC (isothermal conditions)
Radiation field	UVC lamps	Volumetric radiation source emitting at 254 nm, with an output power of 1.4 W	Volumetric radiation source emitting at 254 nm, with an output power of 28.3 W
	Solid walls	Quartz was transparent to UVC at 254 nm with a refractive index of 1.47. Except for the reflector surface, all other surfaces were opaque non-reflective. The reflector was modeled as a specular surface with a reflectivity of 0.89.	Quartz was transparent to UVC at 254 nm with a refractive index of 1.47. Except for the reflector surface, all other surfaces were opaque non-reflective The reflector was modeled as a specular surface with a reflectivity of 0.89.
Species balance	ARZ walls	-	Impermeable (no-flux). Specifically, for the UVC/PDS system, the membrane surface was assumed to emit PDS uniformly and continuously
	PDS mass flow rate emitted by the membrane	-	The mass flow value which, when considering a non-reactive liquid medium, would result in a concentration of 0.6 mM at the outlet

*PDS – Persulfate; **VLX - Venlafaxine

RESULTS AND DISCUSSION

Actinometric tests – Bench-scale tubular membrane photoreactor

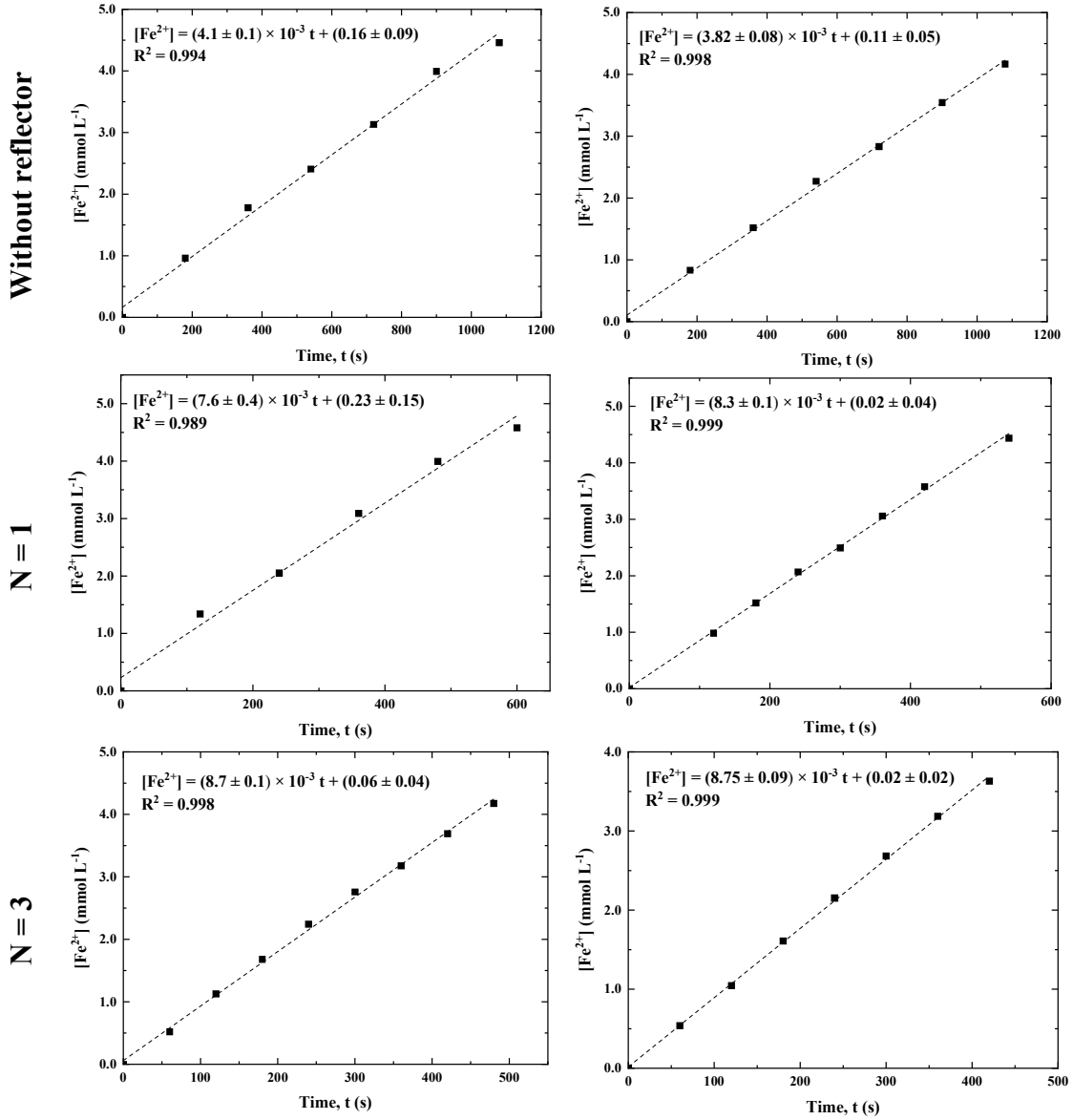

Figure SM-3. Temporal evolution of Fe^{2+} concentration during ferrioxalate actinometry in the bench-scale tubular membrane photoreactor for three reactor configurations: without reflector, N = 1, and N = 3. The experimental data (symbols) and linear regression fits (dashed lines) are shown, with the corresponding slope values representing the Fe^{2+} formation rates and R^2 indicating the quality of the fit. The slopes obtained were used to calculate the incident photon flux for each configuration.

Incident radiation field – Bench-scale tubular membrane photoreactor with N = 3 reflector

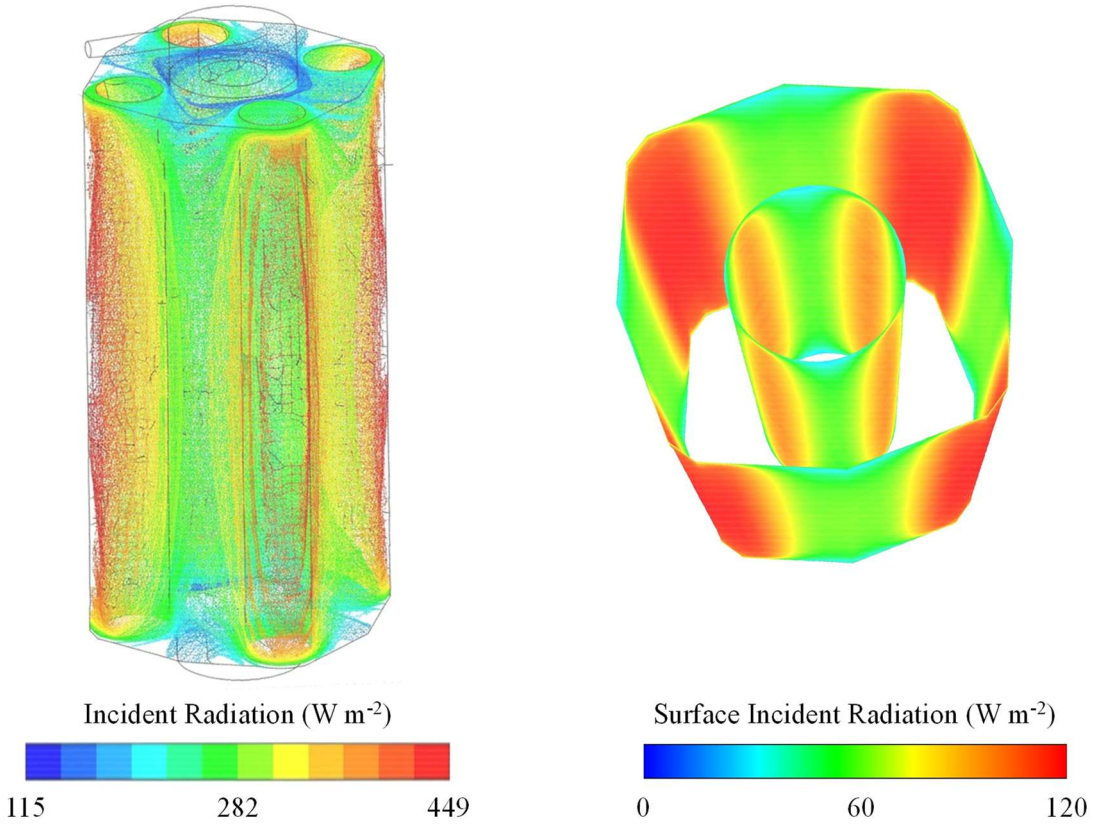

Figure SM-4. Incident radiation field in the bench-scale tubular membrane photoreactor using the N = 3 geometry.

Actinometric tests – Pilot-scale tubular membrane photoreactor

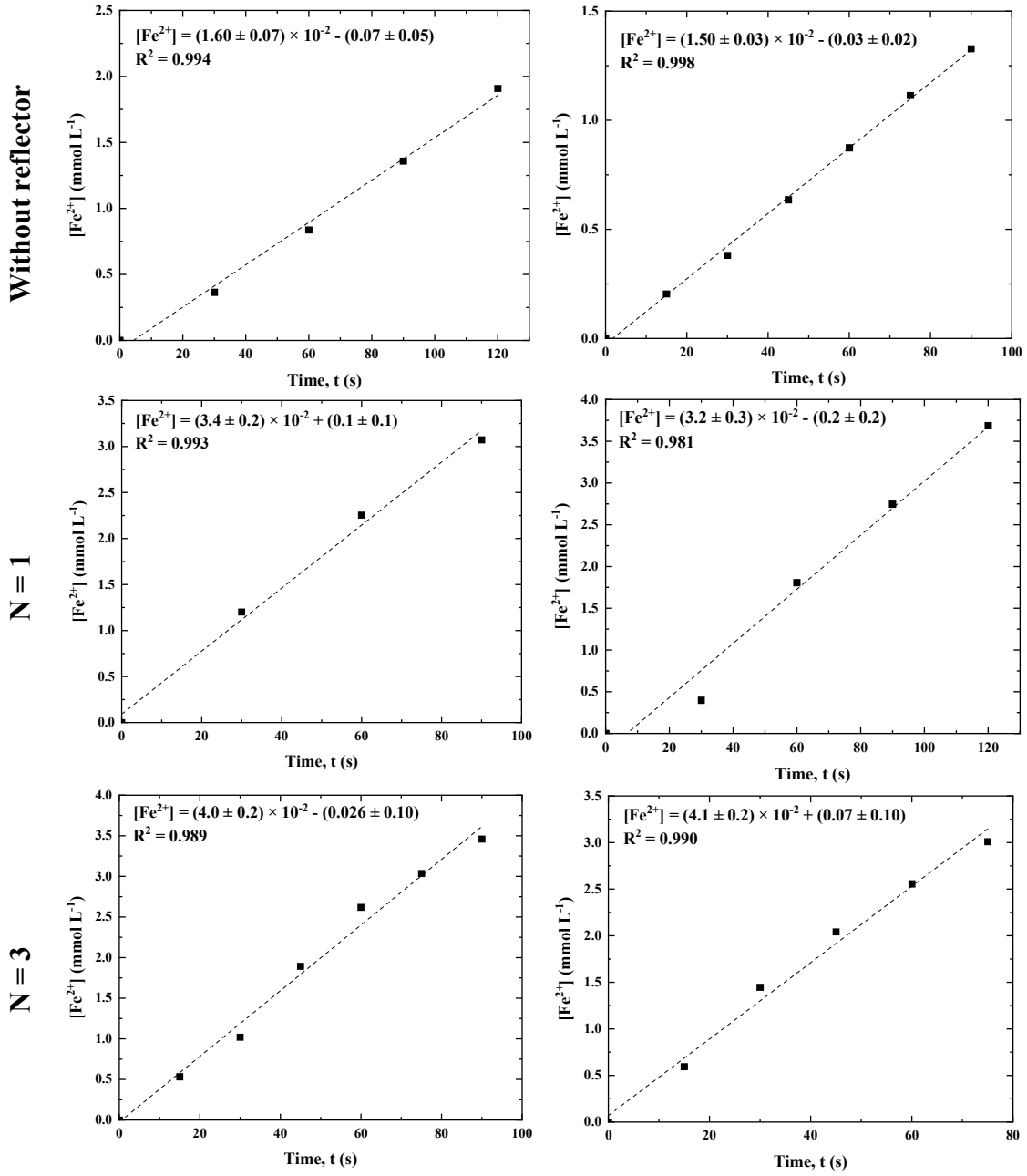

Figure SM-5. Temporal evolution of Fe^{2+} concentration during ferrioxalate actinometry in the pilot-scale tubular membrane photoreactor for three reactor configurations: without reflector, N = 1, and N = 3. The experimental data (symbols) and linear regression fits (dashed lines) are shown, with the corresponding slope values representing the Fe^{2+} formation rates and R^2 indicating the quality of the fit. The slopes obtained were used to calculate the incident photon flux for each configuration

Pilot-scale tubular membrane photoreactor – Photodegradation of VLX with UVC Photolysis: 3D fields of incident radiation, concentration of VLX and $LVRPA_{VLX}$

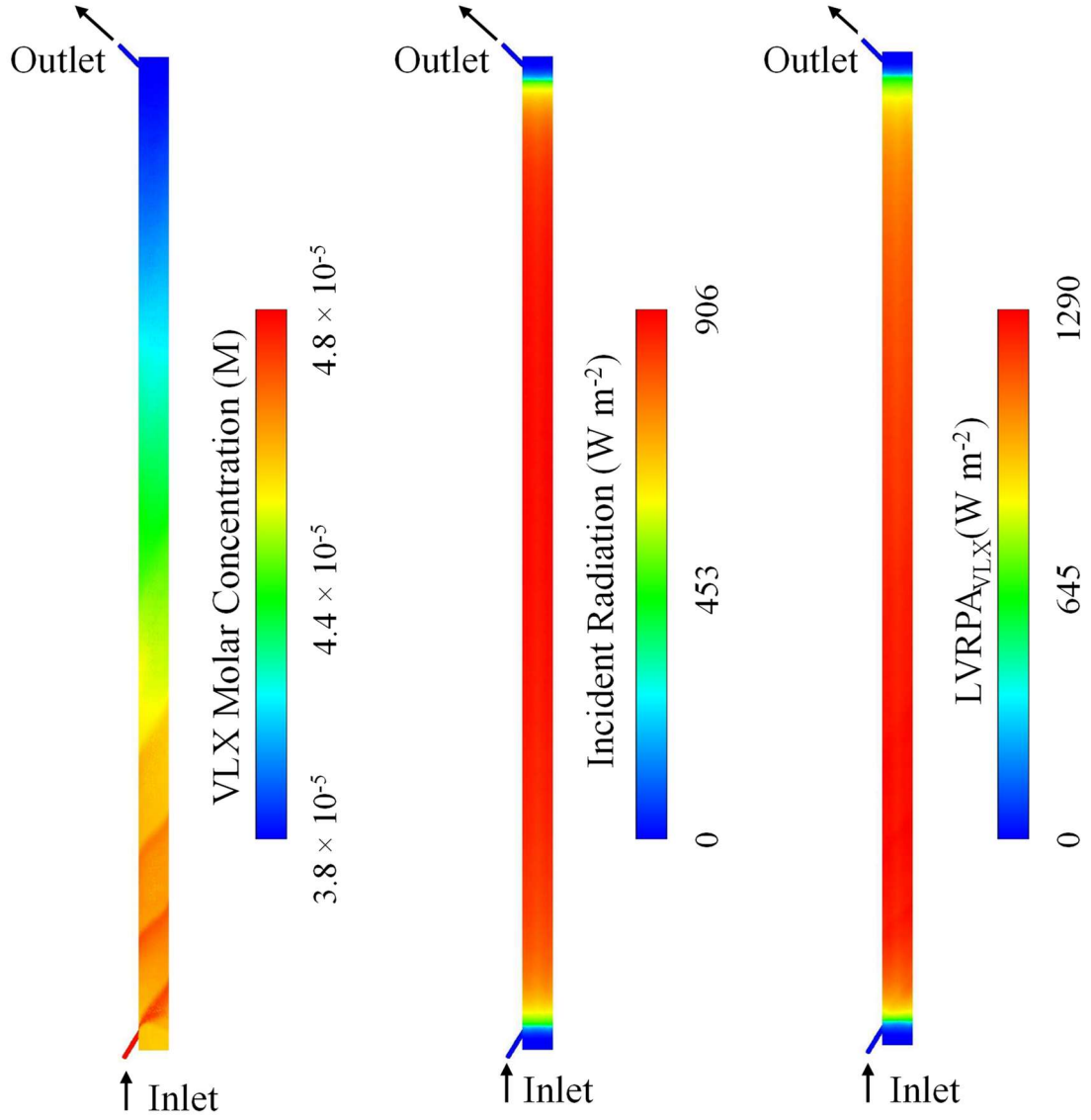

Figure SM-6. 3D fields of incident radiation, concentration of VLX and $LVRPA_{VLX}$ within the pilot-scale tubular membrane photoreactor during the photodegradation of VLX with UVC Photolysis (Exp. #6). Additional operating conditions are detailed in Table 2 of the manuscript.

Permeations tests

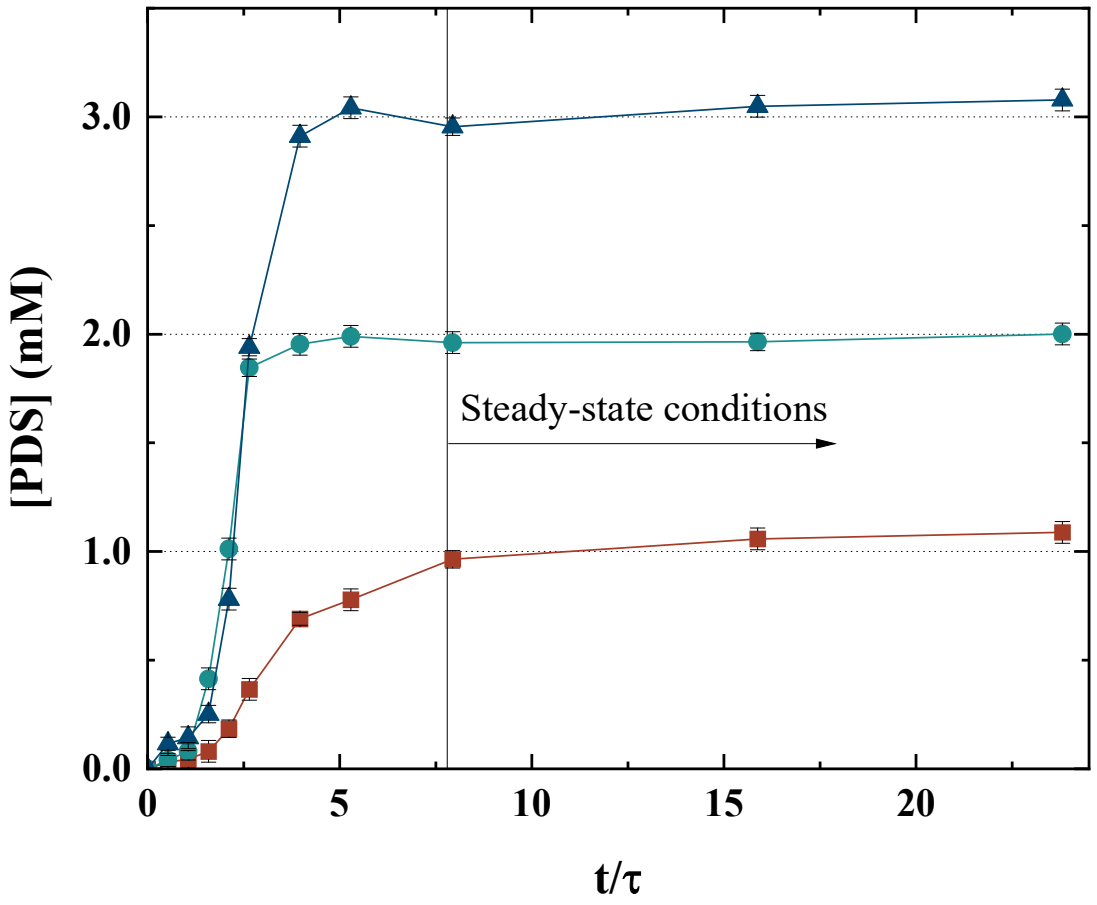

Figure SM-7. PDS concentration profile at the reactor outlet in the absence of radiation for concentrations in the ARZ of 1 mM (■), 2 mM (●), and 5 mM (▲).

Pilot-scale tubular membrane photoreactor – Photodegradation of VLX with UVC/PDS: 3D fields of incident radiation, concentration of VLX and $LVRPA_{VLX}$

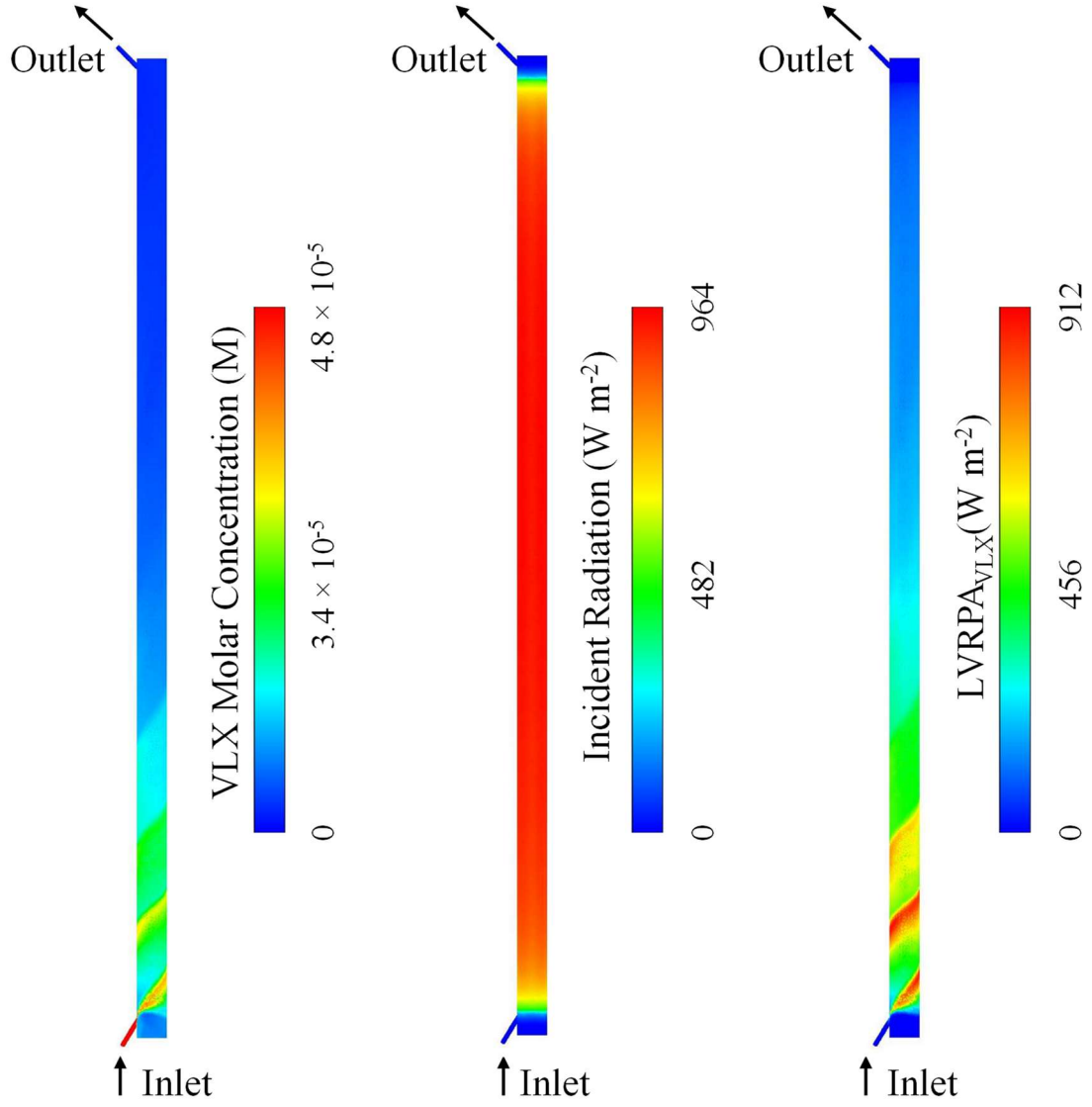

Figure SM-8. 3D fields of incident radiation, concentration of VLX and $LVRPA_{VLX}$ within the pilot-scale tubular membrane photoreactor during the photodegradation of VLX with UVC/PDS (Exp. #9). Additional operating conditions are detailed in Table 2 of the manuscript.

References

[1] M. Martín-Sómer, J. Moreira, C. Santos, A.I. Gomes, J. Moreno-SanSegundo, V.J.P. Vilar, J. Marugán, Reflector design for the optimization of photoactivated processes in tubular reactors for water treatment, Journal of Environmental Chemical Engineering, 11 (2023), 10.1016/j.jece.2023.110609.

[2] APHA, Standard Methods for the Examination of Water and Wastewater (23rd ed.) Washington DC: American Public Health Association., in: A.P.H.A. (APHA) (Ed.), 2017.